Planar circularly symmetric EBG structures for reducing surface wave in printed antennas

Please check the document version of this publication:

• A submitted manuscript is the version of the article upon submission and before peer-review. There can be important differences between the submitted version and the official published version of record. People interested in the research are advised to contact the author for the final version of the publication, or visit the DOI to the publisher's website.
• The final author version and the galley proof are versions of the publication after peer review.
• The final published version features the final layout of the paper including the volume, issue and page numbers.

Link to publication

Planar Circularly Symmetric EBG Structures for Reducing Surface Waves in Printed Antennas

Nuria Llombart, Andrea Neto, *Member, IEEE*, Giampiero Gerini, *Member, IEEE*, and Peter de Maagt, *Senior Member, IEEE*

Abstract—This paper discusses the design and analysis of planar circularly symmetric (PCS) electromagnetic band gap (EBG) structures for reducing the surface waves excited by printed antennas on dense dielectric substrates. The key advantage of the circularly symmetric geometries is that a surface wave generated by a source located at its center experiences the same band gap effect in all radial directions. To obtain simple design rules of the PCS-EBGs for the optimization of the bandwidth, an equivalence is established between 2-D-EBGs and PCS-EBGs. Integrated planar printed antennas with bandwidths up to 20% are designed, manufactured and tested.

Index Terms—Circular structures, dispersion diagrams, electromagnetic band gap (EBG), printed antennas, surface waves.

I. INTRODUCTION

ELECTROMAGNETIC band gap (EBGs) materials [1] are proposed for solving a wide variety of electromagnetic (EM) problems [2]–[5]. However, before EBG technology will be successfully adopted by industry EBG design rules should be made as explicitly as possible and clear and objective (i.e., quantitative) evidence of the advantages of EBG technology is required. In this paper planar structures are considered that are circularly symmetric and radially periodic (PCS-EBG).

The key characteristics of PCS-EBGs are: they are simple to manufacture since they do not present vertical via holes or pins, they do present the same band gap properties for different directions of propagation, and finally, PCS-EBGs can be designed starting from a two-dimensional (2-D) equivalent geometry with a one-dimensional (1-D) periodicity. The 2-D geometry yields a very good first order estimation of the overall performances of the relevant three-dimensional (3-D) geometry, while reducing the numerical effort.

In the field of antennas, center fed circularly symmetric structures have been studied in [6] and [7]. However, circularly symmetric structures have been studied more in depth in the field of Optics and Lasers [8]. Between 1988–1992 the coupled mode theory (CMT) had been used to characterize the performances

of these "diffraction gratings." CMT has been used to show that for large radii of the gratings and small angular variations, i.e., low-order harmonics, the performance of the cylindrically symmetric periodic structures are similar to the equivalent 2-D configurations. This means that there is low TE-TM mode coupling, so that TE and TM properties can be studied separately. This is very intuitive, since for large radii of curvature the cylindrical waves tend to behave as plane waves.

Despite the success in optics, CMT is not the most efficient tool for the design of EBG structures for antenna applications. The reason is that it uses the modes of the unloaded structure (surface waves alone) to represent the overall electromagnetic field configuration in the pseudo-periodic environment. When the pseudo-periodic structures are designed to significantly alter the propagation of surface waves it is more efficient, and intuitive, to adopt a field representation that explicitly includes the periodicity as in Floquet wave expansions.

The dielectric substrates considered in this paper have such a thickness that only the TM_0 mode is in propagation. The design of PCS-EBG is based on the analysis of 2-D-EBGs with 1-D periodicity. These simpler structures are investigated in Section II, using the 2-D-EBGs Green's function that was presented in [9] and using some of the spectral properties outlined in [10]. In particular, the relevant dispersion equations are solved focusing on the complex nature of the eigen value solutions. Based on results of the dispersion equation, design guidelines for monomode EBG configurations are then given. It is shown that the imaginary part of the propagation constant constitutes the key parameter to quantify the effectiveness of an EBG. In Section III the properties of circularly symmetric EBG structures excited by a TM symmetric source are investigated in terms of a continuity of the magnetic field integral equation. A comparison between the magnetic currents in 2-D-EBGs and the ones in the 3-D PCS-EBGs is presented. Based on this comparison the equivalence between 2-D-EBGs and PCS-EBGs is established. Finally, this equivalence, even if demonstrated only in a source symmetric case, is applied in Section IV to a printed antenna. The results demonstrate that 20% bandwidths printed planar antennas that do not excite surface waves can be designed. Finally, in Section V conclusions are drawn.

II. 2-D-EBGs ANALYSIS

In this section, the analysis of 2-D-problems with 1-D periodicities is briefly discussed. The analysis focuses on the dispersion curves with emphasis on the attenuation constant that characterizes the modes inside the band gap, because it constitutes a key design parameter that decides how many loading elements
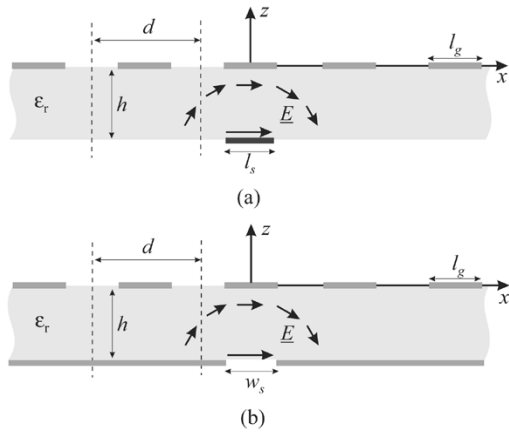
Fig. 1. Geometries under investigation: (a) Dielectric slab loaded by a strip grating and (b) grounded dielectric slab loaded by a strip grating.

Fig. 2. Real and imaginary part of the EBG poles as function of the frequency for ($\epsilon_r = 10$, $h = 5$ mm, $d = 11$ mm, $l_g = 4$ mm).

must be located in the surrounding of an antenna to attenuate the surface wave propagation to a predefined value.

The 2-D basic problems are shown in Fig. 1. Both of them support a TM field configuration and they only differ in the presence or absence of a ground plane. The dielectric layer's constant is ϵ_r, the height of the dielectric is h, while the periodicity is d and the length of the metallic strips is l_g. The procedure to obtain the magnetic currents imposing a continuity of the magnetic field integral equation (CMFIE) in a structure such as in Fig. 1(b), excited by a magnetic source, was described in [11], [12]. More recently, a dual approach to obtain the electric currents by imposing the vanishing of the total electric field in the strip grating of Fig. 1(a) has been presented in [13]. In [9], an EFIE as in [13] and the infinite integral representations of [11], [12] were used to represent the electric currents for both these problems [Fig. 1(a)]. As a result of [9]–[13], the Green's function (GF) of such 2-D problems can be expressed in the spectral domain resorting to the Poisson summation formula. The poles of this GF can be investigated numerically to obtain the propagation constants of the modes that characterize the structure. k is the propagation constant associated to the fundamental space harmonic. When this propagation constant is purely real, the mode is a surface wave propagating in the slab with a phase velocity altered with respect to the one of the unloaded slab. The propagation constant can also be complex. Two different cases are of importance here. When $\text{Re}[k] < k_0$, with k_0 the free space propagation constant, the mode is a leaky wave that radiates in free space and accordingly undergoes an attenuation ($\text{Im}[k] < 0$) as it propagates. When $\text{Re}[k] > k_0$, and $\text{Im}[k] \neq 0$ the mode is in cutoff and the structure is in the band gap region.

Even though this analysis can be performed on arbitrary thickness dielectric slabs, in this paper the attention is limited to thin dielectric slabs. Slabs that, in absence of the periodic loading, support only the TM_0 mode. This allows to track only one pole in the complex plane as a function of the frequency. This is a limitation, but as will be clear at the end of this article, such slabs can host antennas with bandwidths of 20%.

In Fig. 2, the solutions of the dispersion equation k associated to the structure in Fig. 1(a) with parameters ($\epsilon_r = 10$, $h = 5$ mm, $d = 11$ mm, $l_g = 4$ mm) are presented as a function of the frequency. The positive real parts and negative
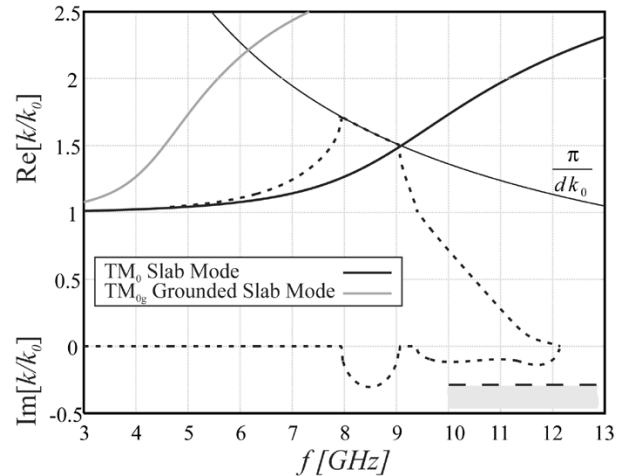
imaginary parts, normalized to k_0, are indicated with dashed lines. The poles are only shown in the Brillouin zone defined by $k \in (-(\pi/d), (\pi/d))$ due to the periodicity of the spectrum ($2\pi m/d$). In Fig. 2, this zone is delimited by a thin curve (explicitly indicated as π/dk_0).

Let us consider two extreme cases. For very large periodicities in terms of the wavelength ($d > \lambda_0$) and very small strips ($l_g < \lambda_0$), the solutions k are essentially the surface waves of the unloaded slab (thick black solid curve). On the other hand, when the period d is small and the strips are large, the solutions tend to be the surface wave of the grounded dielectric slab (thick gray solid curve). Systematically, the solution of the dispersion equation falls between these two extreme configurations. Since the TM_0 slab mode has zero cut off frequency, the poles of the loaded structure emerge from the branch points at $\pm k_0$. As the frequency increases, the poles k tend to π/d. At that frequency point the pole becomes complex, with the real part remaining constant at π/d and with a strong imaginary part. These properties characterize the band gap region. Note that in most cases the dispersion curves are simply interrupted in the correspondence of the band gap, whereas Fig. 2 explicitly quantifies both real and imaginary parts of the mode propagation constant inside the band gap. It should be mentioned that the appearance of the band gap behavior is always associated to the merging of two poles, which in the present case are the one that is being tracked and the *image* arising from the second, ($m = 1$), period $k^1 = -k + (2\pi/d)$. The appearance of a complex propagation constant and its complex conjugate, as it is in the band gap region, can only come from the merging of two roots. This is based on the fact that the number of roots of the dispersion equation cannot change abruptly, except at branch points. In the example of Fig. 2 the band gap extends from 7.95 to 9.05 GHz. The end of the band gap region tends to coincide with the frequency at which the TM_0 slab mode propagates with constant $k_{\text{TM}_0} = \pi/d$. As the frequency ranges from 9.05 to 12.1 GHz, the fundamental space harmonic k becomes faster until it enters the visible (radiating) region and becomes a leaky wave (from 9.41 to 12.1 GHz), since its propagation constant is lower than the one of free space.
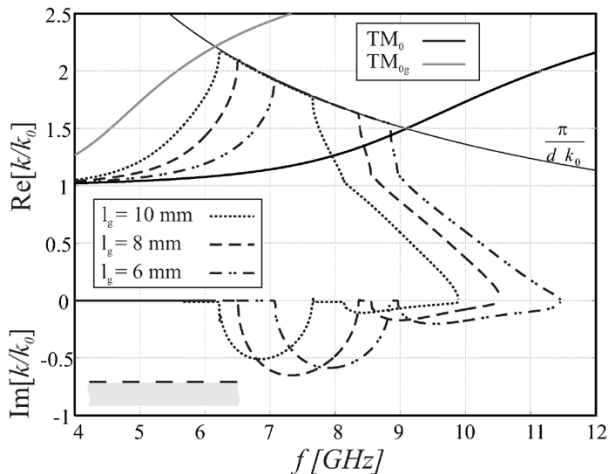
Fig. 3.   Dispersion diagram of the strip loaded dielectric slab with with $\epsilon_r = 10$, $h = 5$ mm, $d = 11$ mm for different strip lengths (l_g).
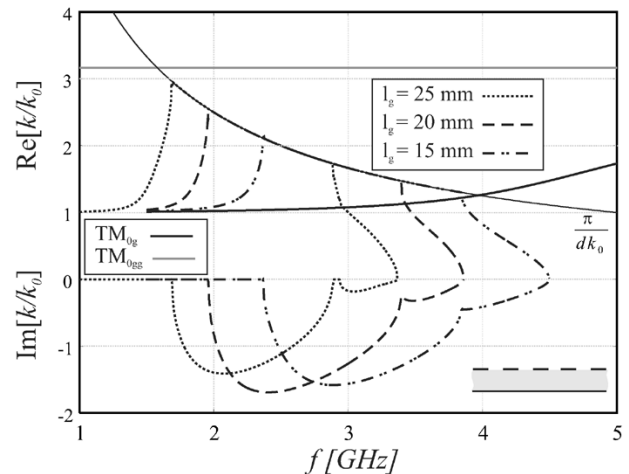

Fig. 4.   Dispersion diagram of a strip loaded grounded dielectric slab with $\epsilon_r = 10$, $h = 5$ mm, $d = 30$ mm for different strip lengths (l_g).

In this article the purpose is to design EBGs associated with high attenuations of the surface wave modes. For this reason only the band gap region is considered.

A. Design Rules

Having described an appropriate way of quantifying the dispersion properties, these curves can be used to guide the design of the EBGs. First, the configuration of Fig. 1(a) will be considered to obtain some general rules. Then the specific advantages associated to the configuration in Fig. 1(b) will be outlined. In the remainder of this section the thickness of the dielectric slab is fixed to 5 mm for the sake of simplicity.

1) Dielectric Slab Loaded by a Strip Grating: Both the position of the band gap and the width of the band gap can be designed acting separately on the only two geometrical parameters available: the periodicity and the strips lengths. The periodicity fixes the position of the Brillouin boundary in frequency. Fig. 3 shows the variation of the band gap for a fixed periodicity of 11 mm and different strip lengths ($l_g = 10$ mm, $l_g = 8$ mm, $l_g = 6$ mm). One can first notice that the band gaps associated to strips closer to the resonance dimensions ($\lambda_{eq} \approx 17$ mm) are wider and present higher attenuation constants, because the strips alter the TM_0 propagation more. The form of the dispersion curves remains essentially the same: they all tend to start after crossing the line that defines the dispersion of the TM_{0g} (grounded slab mode) with the π/dk_0 curve. Moreover, they all tend to end at the crossing with the dispersion curve of the TM_0 (nongrounded slab mode).

As a consequence, the maximum theoretical band gap that can be obtained, for a fixed periodicity, is defined by a curve that unifies the TM_0 and the TM_{0g} dispersion curves while running along the Brillouin zone boundary. It appears that the bandwidth of the EBG structures obtained from a slab with high dielectric constant ($\epsilon_r = 10$) loaded on one side [Fig. 1(a)] is limited to about 25% (in Fig. 3 the max bandwidth is 23.5%).

2) Grounded Dielectric Slab Loaded by a Strip Grating: In order to obtain larger bandwidths, one can resort to a dielectric slab that is grounded on one side and loaded by metallic strips

on the other side [Fig. 1(b)]. The reason why this second structure presents larger bandwidths is that the TM_{0gg} mode (where gg stands for doubly grounded) propagates with phase velocity equal to the homogeneous dielectric one: $k_{TM_{0gg+}} = k_0\sqrt{\epsilon_r}$ while the TM_{0g} mode, at least for low frequencies, propagates with phase velocity similar to the one of free space $k_{TM_{0g+}} = k_0$. This implies that the actual phase velocity of the propagating surface waves can be altered very heavily by the periodic loadings. This is seen in Fig. 4 where π/dk_0 curve in the $Re[k]$-frequency plane follows a longer path that connects the two extreme lines.

Fig. 4 presents some band gaps using the length of the metallic strips ($l_g = 25$ mm, $l_g = 20$ mm, $l_g = 15$ mm) as a parameter. The slab (h, ϵ_r) is the same as in Fig. 3. The periodicity is $d = 30$ mm. The results show that band gaps close to 50% can be achieved by varying the strips length. Such bandwidths are similar to the ones obtainable using vertical pins [4]. One can also observe that the attenuation constants achievable from these structures are generally much larger than those achievable from the nongrounded slabs. A practical consideration is that larger band gaps tend to imply higher attenuation constants. This means that less loading strips are required before achieving the required attenuation of a signal. As an example, the TM_0 mode is attenuated -45.6 dB's at $\lambda_0/2$ distance by the presence of the artificial periodic loading ($l_g = 20$ mm) of Fig. 4 at 2.5 GHz ($\alpha = 1.5k_0$). This means that the mutual coupling between elements printed on the same substrate is only due to space wave coupling. A second advantage of using grounded dielectric slabs as in the antenna designs, is that a clear separation of the radiation half space and the feeding half space is obtained when using electromagnetic coupled patch antennas and the slots are excited via microstrips located on the opposite side of the ground plane.

III. PCS-EBG STRUCTURES

A. TM Symmetric Source

Let us now consider the 3-D-problem of Fig. 5. A reference system is indicated with z-axis normal to the dielectric (ϵ_r) slab of height h that is grounded on one or on both sides. The origin
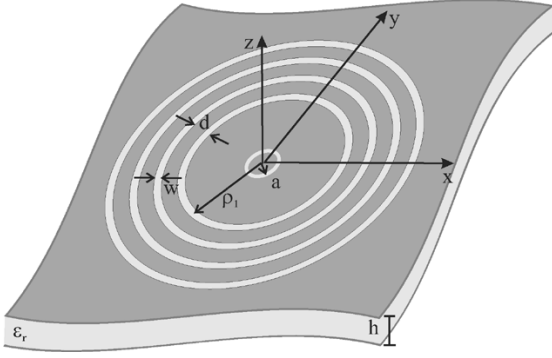
Fig. 5. Circularly symmetric EBG with symmetric magnetic distribution as source.

of the reference system is located on the upper ground plane. A number of concentric rings of slots are etched on the same ground plane, each of them of width w and with radial distances from one to the other being equal to d. The radius of the first periodic ring is ρ_1, so that the array of slots radii are $\rho_n = \rho_1 + (n-1)d$. It is assumed that this structure is excited by an impressed circular magnetic current located around the origin with radius a and that the impressed magnetic current is uniformly distributed along $\mathbf{i}_\phi$. Accordingly, its radiated field will be uniform in ϕ. Clearly, this structure is an inefficient antenna since its broadside radiation pattern is zero. It is, however, instructive to study its behavior to establish the 2-D and PCS-EBG equivalence.

To solve the problem in Fig. 5, it is necessary to derive the magnetic currents in all the apertures of index n given the intensity of the impressed magnetic current. The magnetic field integral equation (CMFIE) can be imposed on the apertures

$$H_\phi^i(\rho) = -H_\phi^s(\rho) \qquad (1)$$

where the superscripts i and s denote incident and scattered fields, respectively. In (1) both the impressed and scattered fields are independent from the angular variable and the entire tangent magnetic field is oriented along $\mathbf{i}_\phi$. Resorting to a standard representation of the fields in cylindrical coordinates [14], the incident (i) and the scattered (s) magnetic fields tangent to the ground plane can be expressed as function of the spectral Green's function. In order to set up a method of moments, the currents on the apertures n are expanded with a set of pulse basis functions j as follows:

$$m_\phi^s(\rho') = \sum_{n=1}^{N} \sum_{j=1}^{M} V_{nj} \frac{1}{\rho'} rect(\rho' - \rho_j - nd, w) \qquad (2)$$

where $rect(x, T) = 1 \,\forall\, |x| < T/2$, and $rect(x, T) = 0 \,\forall\, |x| > T/2$.

A design for the considered structure implies to obtain the width and period of the slotted rings for maximum attenuation of the TM_0 surface wave.

B. Equivalence Between 2-D-EBGS and PCS-EBGS

Limiting the attention to a cross section for constant ϕ of the problem in Fig. 5, a 2-D problem with a 1-D periodicity
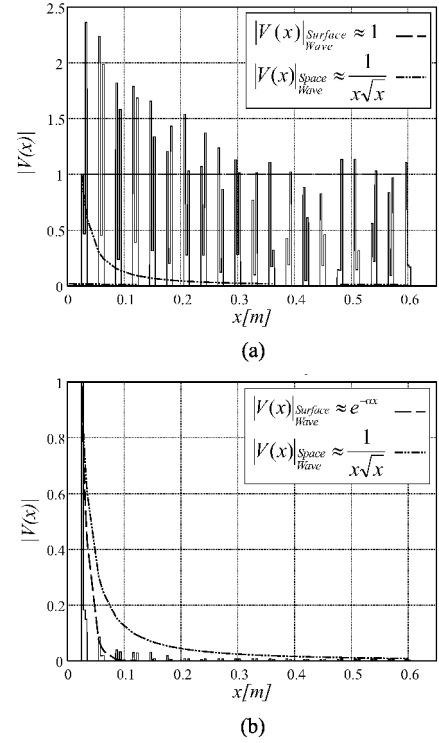

Fig. 6. Normalized magnetic currents amplitudes on the structure of Fig. 1(b) characterized by $\epsilon_r = 10$, $h = 5$ mm, $d = 30$ mm, $w = 10$ mm at (a) $f = 1.8$ GHz outside the band gap and (b) $f = 2.4$ GHz inside the band gap.

is obtained. Moreover, when a line source that provides a TM polarization is considered, an equivalent 2-D-EBG problem is defined. The PCS-EBG is characterized by a cross section as the one in Fig. 1(b), whose dispersion properties have been investigated in Fig. 4 with $l_g = 20$ mm. The band gap associated to the 2-D structure extends from 1.96 to 3.39 GHz (about 53% of relative bandwidth). The maximum attenuation constant ($\approx 1.69k_0$) is observed at 2.4 GHz, whereas at 1.8 GHz the TM_0 is not attenuated, but propagated with propagation constant $1.26k_0$. Both the 2-D-EBG and the PCS-EBG configurations have been analyzed by MoM, where the unknowns are magnetic currents assuming a finite number of apertures in one of the two ground planes, where the width of the apertures is given by $w = l_g - d$. The number of rings for the PCS-EBG is 20 whereas 40 slots have been assumed in the equivalent 2-D-EBG. On each ring or slot, we assumed three pulse basis functions. Fig. 6 shows the amplitude voltage normalized distribution obtained for the 2-D configuration in two cases: a) at $f = 1.8$ GHz outside the band gap b) at 2.4 GHz, inside the bandgap. An arbitrary normalization has been used such that the amplitude of the first basis function on the first array element is set to one. One can clearly observe that when the TM_0 mode is propagating [Fig. 6(a)], it is also dominant since it is not attenuated, and it has a plane wave behavior propagating with constant amplitude. The oscillations in the magnetic current is due to the interference associated to an end-point contribution. Instead, when the mode is not propagating [Fig. 6(b)], the decay of the magnetic currents is mostly exponential. However, the contributions from the space wave should also be accounted for. These latter present a $1/x^{3/2}$ decay as shown in [10].
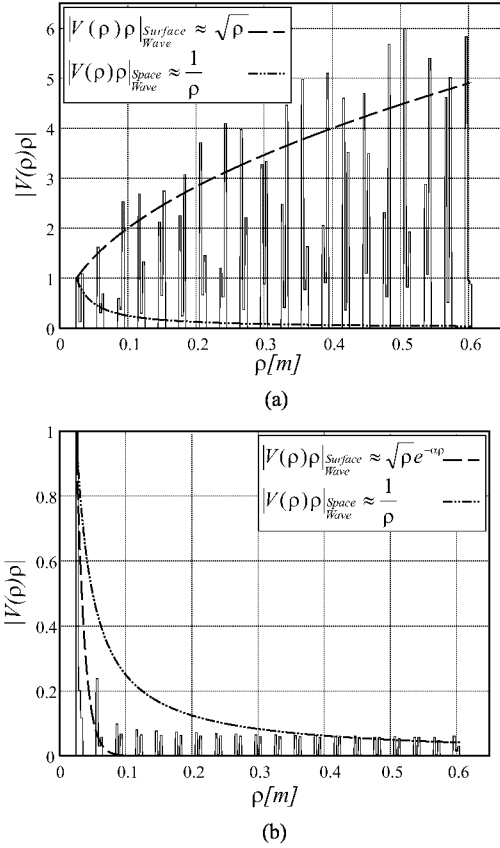
Fig. 7. Normalized magnetic currents amplitudes for the CS-EBG characterized by $\epsilon_r = 10$, $h = 5$ mm, $d = 30$ mm, $w = 10$ mm, $a = 30$ mm at (a) $f = 1.8$ GHz outside the band gap and (b) $f = 2.4$ GHz inside the band gap.

Fig. 7 shows the normalized amplitude voltage distribution obtained for the PCS-EBG configuration in the same two frequencies. For this 3-D problem the voltages are the ones defined in (2) (note the $1/\rho$ scaling factor). When the mode is propagating, Fig. 7(a), it is also dominant as in the 2-D case, but it has a cylindrical wave behavior $e^{-jk_{sw}\rho}/\sqrt{\rho}$. Accordingly, this means that the weights V_n in (2) grow as $e^{-jk_{sw}\rho}\sqrt{\rho}$. Fig. 7(b) shows that in the 3-D case, the currents inside the band gap also decay exponentially and are dominated by the space wave contribution.

From the analysis of these results at arbitrary frequencies inside or outside the band gaps one can deduce that the presence of a band gap from the TM_0 propagation in a 2-D-EBG case implies its existence in a PCS-EBG as well. The major differences are in the following spreadings.

1) A plane wave behavior in the equivalent structure corresponds to a cylindrical spreading in the CS structure.
2) A cylindrical spreading in the equivalent structure implies a $1/\rho$ in the CS structure.

IV. PRINTED ANTENNA

The antenna considered in this section is shown in Fig. 8. It consists of two dielectric slabs with the same dielectric constant ϵ_r and different heights h and h_m divided by a ground plane. There is a slot etched in the ground plane of dimensions l_s and w_s. The slot is coupled to an orthogonal dipole (l_d and w_d) located on the top of the upper dielectric slab h. Finally, the
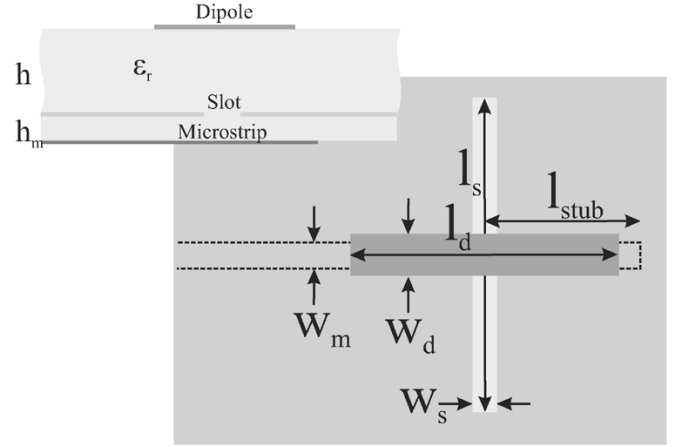

Fig. 8. Side and top view of the printed antenna: Slot (l_s, w_s) coupled to a dipole (l_d, w_d) and excited via microstrip (l_{stub}, w_m).

structure is excited via a microstrip of dimensions l_{stub} and w_m printed on the other side of the lower dielectric slab h_m.

Printed antennas present one key disadvantage: small bandwidth over which high efficiency is obtained. In practice, the height of the substrate on which the dipole is printed h dominates the bandwidth and efficiency. Beyond a certain substrate height, the antenna starts to generate a dominant surface wave field. The bandwidth achieved from this type of antenna configurations with a limited substrate thickness and dielectric constant of $\epsilon_r = 10$, and without any dedicated optimization is about 12%. Nevertheless, 60–70% of the power delivered by the source [15] is launched into the TM_0 mode. The design rules that were shown in Section II-A will be used to improve the efficiency of such antennas.

A. PCS-EBG: Nonsymmetric Source

In Section III a symmetric TM source was assumed, which generated only a pure TM field with the electric field entirely polarized along ρ. When the source is not symmetric, it generates electric field components in both ρ and ϕ directions. If one was simply to use the rings that were previously introduced, they would support azimuthal electric currents that can lead to strong resonances. Such strong resonances in the azimuthal direction can be responsible for a significant alteration of the input impedance and thus lead to a bandwidth reduction. However, for large values of ρ, the electric field associated to the TM surface waves presents an electric field with only the ρ component.

In order to demonstrate this, the transverse electric field in cylindrical coordinates excited by an elemental slot $m(x', y', zs) = \delta(x', y', zs)\mathbf{i}_y$ oriented along y into a dielectric slab can be calculated using Green's function formalism, [14], as

$$\mathbf{E}(\rho, \phi, z) = -\frac{1}{8\pi}(I_1 - I_2)\cos(\phi)\mathbf{i}_\rho$$
$$+ \frac{1}{8\pi}(I_1 + I_2)\sin(\phi)\mathbf{i}_\phi$$

where

$$I_1 = \int_{-\infty}^{\infty}(V_{\text{TM}}(z) + V_{\text{TE}}(z))H_0^2(k_\rho\rho)k_\rho dk_\rho \tag{3}$$

$$I_2 = \int_{-\infty}^{\infty}(V_{\text{TM}}(z) - V_{\text{TE}}(z))H_2^2(k_\rho\rho)k_\rho dk_\rho. \tag{4}$$
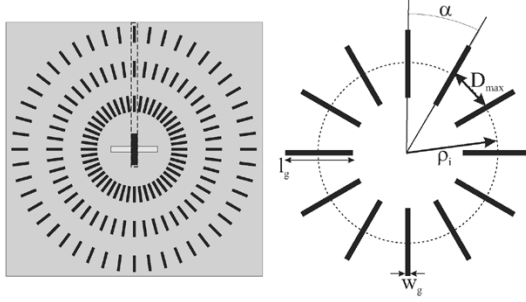
Fig. 9.   Geometrical parameters of a single ring of radial dipoles.

$V_{\mathrm{TM}}(z)$ and $V_{\mathrm{TE}}(z)$ are the voltage solutions due to a series unit voltage generator in the equivalent TM and TE transmission lines of the dielectric stratification.

Since only one TM mode is in propagation, the ρ component of the electric field depends on the difference of the Hankel functions of order 0 and 2. Meanwhile, the ϕ component of **E** depends on the sum of the same functions. Using the asymptotic expression for large argument of the Hankel functions [14], it results $H_0^2(k_\rho\rho) + H_2^2(k_\rho\rho) \approx 0$ and $H_0^2(k_\rho\rho) - H_2^2(k_\rho\rho) \approx 2\sqrt{(2/\pi)}\left(e^{-jk_\rho\rho}e^{j(\pi/4)}/\sqrt{k_\rho\rho}\right)$ for $k_\rho\rho \gg 1$. As the ϕ component of the electric field depends on the sum of the hankel functions, the electric field has asymptotically only the ρ component. The same applies to the electric field generated by a dipole at the dielectric-air interface. Applying similar considerations, one can show that the electric field associated to TE waves launched by a central source is asymptotically oriented only along ϕ.

Thus, a simple modification of the PCS-EBG configuration can be applied resorting to dipoles oriented in the radial direction around the source. The radial dipoles will only act on the ρ component of the electric currents (or of the electric fields), thus they will not introduce additional resonances. In terms of suppression of the TM surface wave, the radial dipoles behave almost exactly the same as the continuos rings.

In Fig. 9 the geometrical parameters of this new configuration are shown. The radial position $\rho_i = \rho_1 + (i-1)d$ and length l_g can be designed using the same equivalent 2-D-EBG model as before. Only now, there are two additional parameters, the width of the dipoles w_g and the angle at which the dipoles are placed α (it defines the number of dipoles per ring). Simulations have shown that the influence of w_g is small, whereas the angle α has to be chosen so that the TM_0 mode still experiences a continuous surface. In terms of array theory this implies that each wave front that has normal incidence must encounter elements that are sampled in ϕ, at least at the Nyquist frequency: $D_{\max} \le (\lambda_{\mathrm{TM0}}/2) \le (\pi/k_{\mathrm{TM0}})$, where k_{TM0} is the propagation constant of the TM_0 mode of the grounded slab.

B. Surface Wave Coupling Reduction

In order to quantify the effect of the EBG structure on the performances of the antenna in Fig. 8, a panel composed of six printed antennas has been built (Fig. 10). Two of these antennas are surrounded by a PCS-EBG consisting of two or three rings. The other four antennas are simple printed antennas. The parameters l_g and d from the PCS-EBG are designed using the 2-D model described in Section II, in order to obtain a band gap
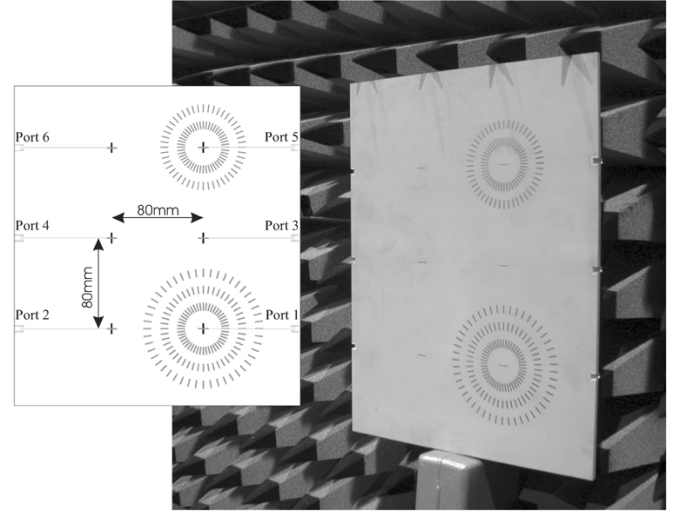

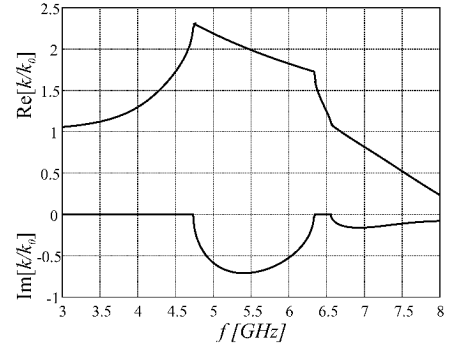Fig. 10.   Panel with six antennas located in a square grid of 80 mm.

Fig. 11.   Dispersion diagram for a grounded slab with parameters $\epsilon_r = 10$ and $h = 3.81$ mm loaded by a strip grating of $d = 13.7$ mm and $l_g = 6.6$ mm.

in the frequency band of interest (see the 2-D dispersion diagram in Fig. 11).

Fig. 12 shows the S-parameters of the antennas without EBG. The measurements are compared with the simulations done using Ansoft Designer. One can first note that the single element impedance bandwidth ($S_{33} < -10$ dB) is in the order of 12%. The S_{34} case in which the antennas are situated at a distance of 80 mm in the maximum coupling direction, is around -17 dBs. The second parameter S_{36} is around -23 dB and corresponds to case where the antennas are placed at a 45° angle from one to the other. For both these configurations the coupling is essentially due to the TM_0 surface wave.

The PCS-EBG implemented in the prototype is designed using the 2-D design rules shown in Section II-A, starting from the grounded slab and aimed at achieving the band gap in the frequency band from 4.75 to 6.4 GHz (29.6%). The parameters that define the appropriate 2-D-EBG are ($l_g = 6.6$ mm, $d = 13.7$ mm). Once the EBG periodicity and the dipole length are defined in such a way, the remaining degrees of freedom are only the width of the dipoles w_g and the distance ρ_1 (Fig. 9). The first has a secondary role and can be used for tuning the EBG band. The second, however, can be used to enhance the matching between the input impedance of the antenna and the micro-strip line. Fig. 13 shows the S-parameters related to the antenna with the two rings EBG surrounding it.
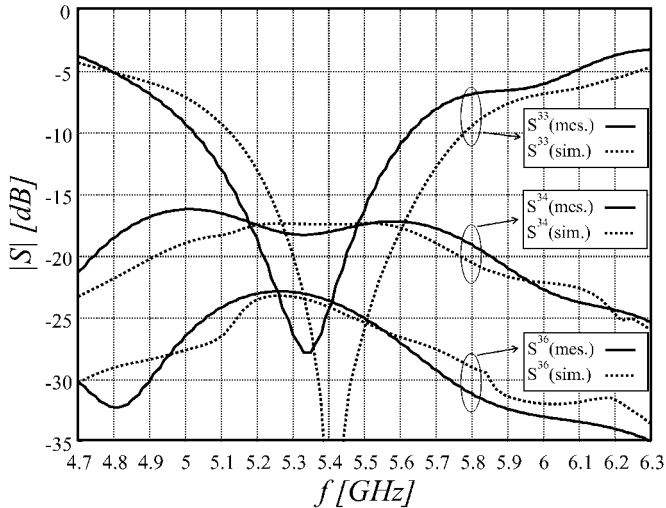
Fig. 12. S-parameters pertinent to simple antennas ($l_s = 8.5$ mm, $w_s = 1$ mm, $l_d = 8.25$ mm, $w_d = 0.6$ mm, $l_{\text{stub}} = 4.3$ mm, $w_m = 0.37$ mm) printed on a substrate with parameters $\epsilon_r = 10$, $h = 3.81$ mm and $h_m = 0.381$ mm.
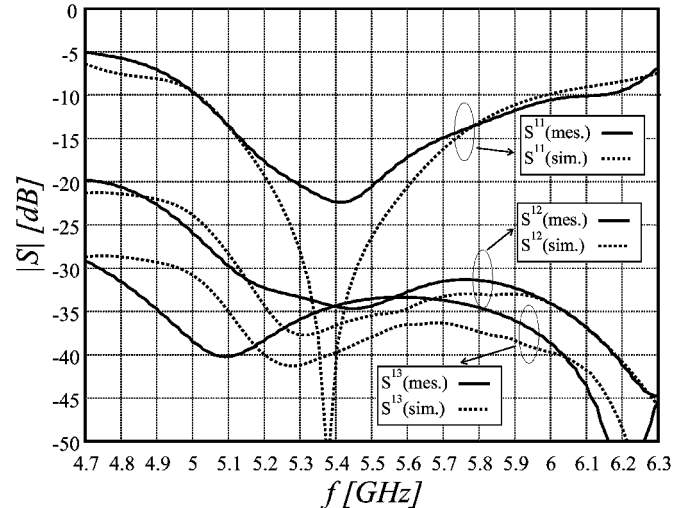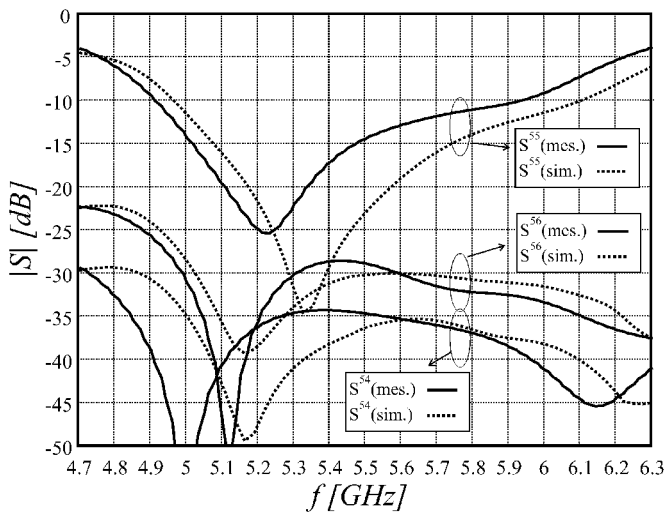

Fig. 13. S-parameters pertinent to the antenna surrounded by two rings of dipoles ($l_s = 8.5$ mm, $w_s = 1$ mm, $l_d = 8.25$ mm, $w_d = 0.75$ mm, $l_{\text{stub}} = 3.8$ mm, $w_m = 0.37$ mm, $\rho_1 = 18$ mm, $d = 13.7$ mm, $l_g = 6.6$ mm, $\alpha = 7.5°$).

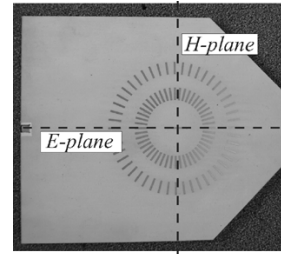The S_{55} parameter of the antenna surrounded by the EBG is improved so that the impedance bandwidth has increased to 20%. Most importantly, there is also a significant reduction of the coupling between antennas. The S_{56} parameter is in the order of -30 dBs. Finally, the results pertinent to the same configuration, but using an EBG based on three rings, are shown in Fig. 14. It should be noticed that the third ring does not significantly improve the isolation between the antennas. This is due to the fact that the space wave contribution is always present and dominates the coupling when the surface waves have been eliminated.

Finally, it can be pointed out that the agreement between calculated (Ansoft Designer) and measured results is good. The slight different central resonant frequency of the antennas is associated to the uncertainty of the dielectric constant provided by the manufacturer.

Fig. 14. S-parameters pertinent to the antenna surrounded by three rings of dipoles (geometrical parameters of Fig. 13).

Fig. 15.   Panel portion containing the antenna surrounded by two rings.

C. Radiation Pattern

In order to perform the measurements and obtain a fair comparison between the performances of the three different antenna configurations (no EBG, two rings EBG and three rings EBG) the panel has been cut in portions of the same dimension. The result is that three small subpanels, with one antenna each, were obtained. A photograph of one of these panels is shown in Fig. 15. Also, the E-and H-plane cuts are shown in the same figure. The measurements were then performed in the cylindrical near field scanning facility at TNO.

Fig. 16 shows the co-polar radiation patterns in the E-plane and H-plane measured at the central frequency ($f = 5.4$ GHz) for all three antennas considered. All curves are normalized to their maximum values. Observing the H-plane first, one can notice a very significant difference between the 3 dB angle obtained with and without EBGs. Especially in absence of EBGs the surface wave diffraction at the edges of the substrate heavily affects the actual radiation patterns. It appears that the two ring antenna presents narrower beams and thus higher directivity than the three rings one. This might come as a surprise since the effective area of the antenna is larger in the latter case. However, the phase and amplitude distribution in the dipoles composing the rings is not constant. For certain frequency ranges the third ring appears to be contributing in counter phase with respect to the central antenna and the first two rings. The three rings antenna radiation pattern is generally more frequency dependent than the two ring one.
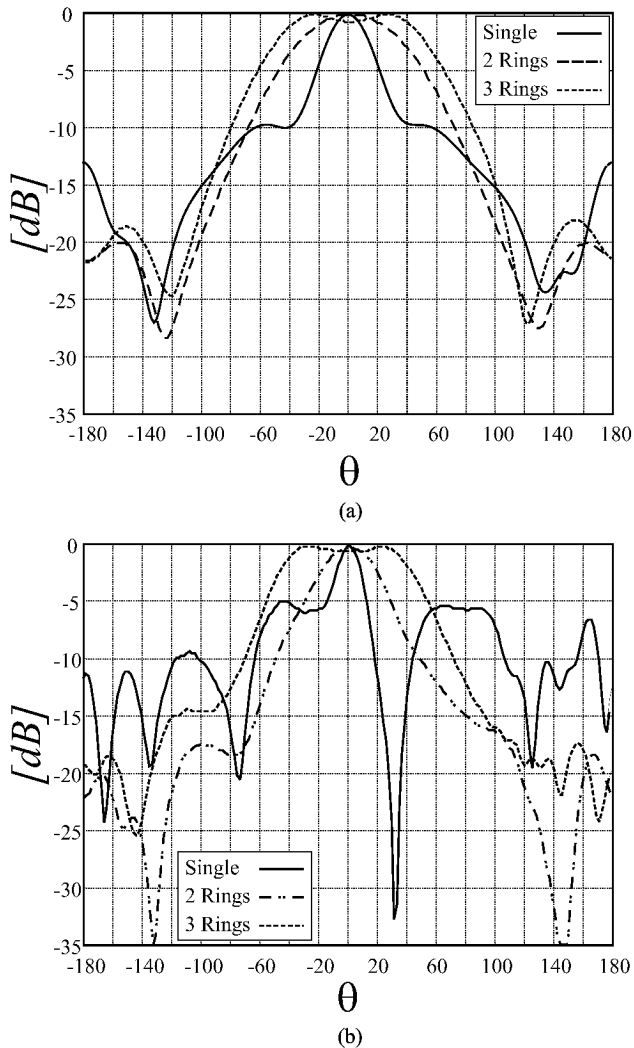
(a)

(b)

Fig. 16.   H-plane (a) and E-plane (b) radiation patterns for the single antenna, the PCS-EBG antenna with two rings and three rings.

Fig. 16(b) finally shows the measured radiation patterns pertinent to the E-plane. In this case, the patterns are generally not symmetric, due to the asymmetry of the slab structures. Most importantly, the impact of surface wave diffraction on the single antenna pattern is significant with a first deep null well inside the 3 dB radiation pattern zone.

It is worth noting that the radiation patterns in the E-plane are asymmetric due to the presence of the connectors. These latter seem to introduce a radiated contribution, which is visible in the back half space at levels lower than 15 dBs with respect to the maximum. Nevertheless, from both the E and the H-plane measurements it is clear that the front to back ratio has improved.

The same isolated antennas have been simulated with Ansoft Designer, which considers an infinite substrate (no edge effects). The gain given by this tool can be interpreted as a measure of the radiation efficiency of the antenna. Fig. 17 shows the gains for the three antennas at broadside and at backside as a function of the frequency. In the presented designs, the antenna without EBG has a very low gain due to the fact that more than 60% of the power is launched into the TM_0 surface wave and the diffraction at the edge of the substrate is not accounted for. How-
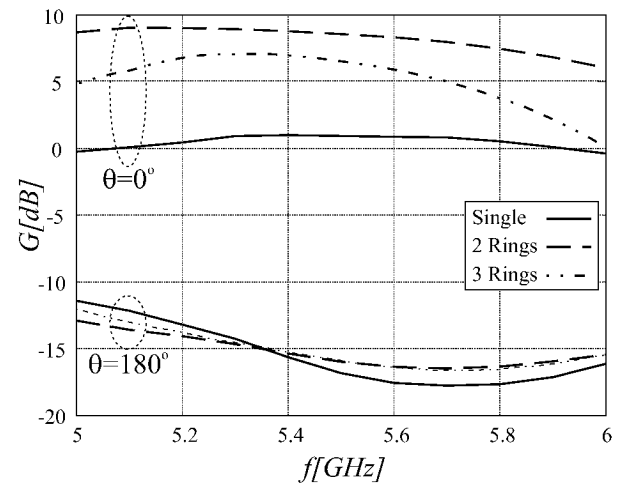

Fig. 17.   Gain at $\theta = 0°$ and $\theta = 180°$ for the single antenna, the PCS-EBG antenna with two rings and three rings.

ever, even if real gain, including edge effects, turns out to be higher, it is not controllable, thus it cannot be used. When the antenna is simulated with the two rings PCS-EBG around it, a significant gain improvement of around 8.5 dBs is observed. Already with two rings a surface wave efficiency of 90% is obtained, which corresponds to 3 dBs of gain improvement. The additional gain improvement is associated to a larger effective area of the antenna. For the three rings case, around 6 dBs of gain improvement is obtained, but the gain of the three rings case is much more frequency dependent, as explained before. In conclusion, two rings seem to be sufficient to suppress the surface wave and maintain a clean radiation pattern over a broad band.

V. Conclusion

In this paper, the use of purely planar circularly symmetric periodic metallic loadings has been proposed to impede the propagation of the TM_0 in planar printed structures. Some advantages are obtained using these sort of structures. First, they are planar and thus not difficult to manufacture. Secondly, the surface wave propagation is reduced in all radial directions, thanks to the circular symmetry. Finally, the design of these structures is simple, since it is based on the solution of 2-D problem and extension to 3-D geometries. The main advantage of the design simplicity is that the performances of the ensemble of antenna and EBG can be easily optimized to meet specific requirements. In the example presented in this paper the emphasis was on bandwidth. An antenna with 20% of bandwidth has been presented that does not suffer from surface wave effects. Different tradeoffs can easily be performed to achieve specific requirements.

Acknowledgment

References

[1] E. Yablonovitch, "Inhibited spontaneous emission in solid state physics and electronics," *Phys. Rev. Lett.*, vol. 58, no. 20, pp. 2059–2062, May 1987.

[2] P. de Maagt, R. Gonzalo, Y. C. Vardaxoglou, and J. M. Baracco, "Electromagnetic bandgap antennas and components for microwave and (Sub)millimeter wave applications," *IEEE Trans. Antennas Propag.*, vol. 51, no. 10, pp. 2667–2677, Oct. 2003.

[3] R. Gonzalo, P. de Maagt, and M. Sorolla, "Enhanced patch antenna performance by suppressing surface waves using photonic band gap substrates," *IEEE Trans. Microw. Theory Tech.*, vol. 47, no. 11, pp. 2099–2104, Nov. 1999.

[4] D. Sievenpiper, L. Zhang, R. F. Broas, N. G. Alexopolous, and E. Yablonovitch, "High-impedance electromagnetic surfaces with a forbidden frequency band," *IEEE Trans. Microw. Theory Tech.*, vol. 47, no. 11, pp. 2059–2074, Nov. 1999.

[5] R. Coccioli, F.-R. Yang, K.-P. Ma, and T. Itoh, "Aperture-coupled patch antennas on UC-PBG," *IEEE Trans. Microw. Theory Tech.*, vol. 47, no. 11, pp. 2123–2130, Nov. 1999.

[6] E. Lier and P. S. Kildal, "Soft and hard horn antenna," *IEEE Trans. Antennas Propag.*, vol. 36, no. 11, pp. 1152–1157, Nov. 1988.

[7] Z. Ying, P. S. Kildal, and A. A. Kishk, "Study of different realizations and calculation models for soft surfaces by using vertical monopole on a soft disk as a test bed," *IEEE Trans. Antennas Propag.*, vol. 44, no. 11, pp. 1474–1481, Nov. 1996.

[8] C. Wu, T. Makino, R. Maciejko, S. I. Najafi, and M. Svilans, "Simplified coupled-wave equations for cylindrical waves in circular grating planar waveguides," *IEEE J. Lightwave Tech.*, vol. 10, no. 11, pp. 1575–1589, Nov. 1992.

[9] N. Llombart, A. Neto, G. Gerini, and P. de Maagt, "Periodic structures excited by non periodic structures," in *Proc. 27th ESA/ESTEC Workshop on Innovative Periodic Antennas*, Mar. 2004, pp. 601–607.

[10] F. Capolino, D. R. Jackson, and D. R. Wilton, "Fundamental properties of the field at the interface between air and a periodic artificial material excited by a line source," *IEEE Trans. Antennas Propag.*, vol. 53, no. 1, pp. 91–99, Jan. 2005.

[11] R. A. Sigelmann and A. Ishimaru, "Radiation from periodic structures, excited by an aperiodic source," *IEEE Trans. Antennas Propag.*, no. 3, pp. 354–364, May 1965.

[12] R. A. Sigelmann, "Surface waves on grounded dielectric slab covered by a periodically slotted conducting plane," *IEEE Trans. Antennas Propag.*, no. 5, pp. 672–676, Sep. 1967.

[13] H. Y. D. Yang and D. R. Jackson, "Theory of line-source radiation from a metal-strip grating dielectric-slab structure," *IEEE Trans. Antennas Propag.*, vol. 48, no. 4, pp. 556–564, Apr. 2000.

[14] L. Felsen and N. Marcuvitz, *Radiation and Scattering of Waves*. New York: IEEE Press, 1994.

[15] S. F. Mahmoud, Y. M. M. Antar, H. F. Hammad, and A. P. Freundorfer, "Theoretical considerations in the optimization of surface waves on a planar structure," *IEEE Trans. Antennas Propag.*, vol. 52, no. 8, pp. 2057–2063, Aug. 2004.

Andrea Neto (M'00) received the laurea degree (*summa cum laude*) in electronic engineering from the University of Florence, Florence, Italy, in 1994 and the Ph.D. degree in electromagnetics from the University of Siena, Siena, Italy, in 2000.

Part of his Ph.D. was developed at the European Space Agency Research and Technology Center, Noordwijk, The Netherlands, where he worked in the Antenna Section for two years. In 2000 to 2001, he was a Postdoctoral Researcher at the S.W.A.T. Group of the Jet Propulsion Laboratory, California Institute of Technology, Pasadena. Since 2002, he is a Senior Antenna Scientist at TNO Defence, Security and Safety, Den Haag, The Netherlands.

His research interests are in the analysis and design of antennas, with emphasis on arrays, dielectric lens antennas, wide band antennas and EBG structures.

Giampiero Gerini (M'92) received the M.S. degree (*summa cum laude*) and the Ph.D. degree in electronic engineering from the University of Ancona, Ancona, Italy, in 1988 and 1992, respectively.

From 1994 to 1997, he was Research Fellow at the European Space Research and Technology Centre (ESA-ESTEC), Nooordwijk, The Netherlands, where he joined the Radio Frequency System Division. Since 1997, he has been with the Netherlands Organization for Applied Scientific Research (TNO), The Hague, The Netherlands. At TNO Defence, Security and Safety, he is currently Chief Senior Scientist of the Antenna Unit in the Transceivers and Real-time Signal Processing Department. His main research interests are phased array antennas, frequency selective surfaces, and integrated front-ends.

Nuria Llombart received the Ingeniero de Telecomunicación degree from the Universidad Politécnica de Valencia, Spain, in 2002. She is working toward the Ph.D. degree at the same university.

She spent one year, 2000 to 2001, at the Friedrich-Alexander University of Erlangen-Nuremberg, Germany, and worked at Fraunhofer Institute for Integrated Circuits in Erlangen, Germany, from 2000 until 2002. Her current research interests include numerical and analytical methods for the analysis and design of printed antennas and EBG structures.
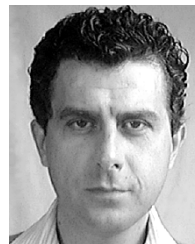
Ms. Llombard Ph.D. studies are financed and hosted by the Defence, Security and Safety Institute of the Netherlands Organization for Applied Scientific Research (TNO) in The Hague, The Netherlands.

Peter de Maagt (S'88–M'88–SM'02) was born in Pauluspolder, The Netherlands, in 1964. He received the M.Sc. and Ph.D. degrees from Eindhoven University of Technology, Eindhoven, The Netherlands, in 1988 and 1992, respectively, both in electrical engineering.

He is currently with the European Space Research and Technology Centre (ESTEC), European Space Agency, Noordwijk, The Netherlands. His research interests are in the area of millimeter and submillimeter-wave reflector and planar integrated antennas, quasioptics, photonic bandgap antennas, and millimeter- and submillimeter-wave components.

Dr. de Maagt was co-recipient of the H.A. Wheeler Award of the IEEE Antennas and Propagation Society for the Best Applications Paper of 2001. He was granted a European Space Agency Award for innovation in 2002.